

Wavefront detection method of a single-sensor based adaptive optics system

Chongchong Wang,^{1,2} Lifa Hu,^{1,*} Huanyu Xu,¹ Yukun Wang,¹ Dayu Li,¹ Shaoxin Wang,¹ Quanquan Mu,¹ Chengliang Yang,¹ Zhaoliang Cao,¹ Xinghai Lu,¹ and Li Xuan¹

¹State Key Laboratory of Applied Optics, Changchun Institute of Optics, Fine Mechanics and Physics, Chinese Academy of Sciences, Changchun, Jilin 130033, China

²Chinese Academy of Sciences University, Beijing 100039, China

*hulifa@ciomp.ac.cn

Abstract: In adaptive optics system (AOS) for optical telescopes, the reported wavefront sensing strategy consists of two parts: a specific sensor for tip-tilt (TT) detection and another wavefront sensor for other distortions detection. Thus, a part of incident light has to be used for TT detection, which decreases the light energy used by wavefront sensor and eventually reduces the precision of wavefront correction. In this paper, a single Shack-Hartmann wavefront sensor based wavefront measurement method is presented for both large amplitude TT and other distortions' measurement. Experiments were performed for testing the presented wavefront method and validating the wavefront detection and correction ability of the single-sensor based AOS. With adaptive correction, the root-mean-square of residual TT was less than 0.2λ , and a clear image was obtained in the lab. Equipped on a 1.23-meter optical telescope, the binary stars with angle distance of $0.6''$ were clearly resolved using the AOS. This wavefront measurement method removes the separate TT sensor, which not only simplifies the AOS but also saves light energy for subsequent wavefront sensing and imaging, and eventually improves the detection and imaging capability of the AOS.

©2015 Optical Society of America

OCIS codes: (010.1080) Active or adaptive optics; (010.7350) Wave-front sensing.

References and links

1. J. W. Hardy, *Adaptive Optics for Astronomical Telescopes* (Oxford U. Press, 1998).
2. F. Roddier, *Adaptive Optics in Astronomy* (Cambridge U. Press, 1999).
3. R. Tyson, *Principles of Adaptive Optics* (CRC Press, 2010).
4. W. Jiang, N. Ling, G. Tang, M. Li, F. Shen, C. Rao, Y. Zhu, and B. Xu, "61-element adaptive optical system for 1.2-m telescope of Yunnan Observatory," *Proc. SPIE* **3353**, 696–703 (1998).
5. M. A. van Dam, D. Le Mignant, and B. A. Macintosh, "Performance of the Keck Observatory adaptive-optics system," *Appl. Opt.* **43**(29), 5458–5467 (2004).
6. J.-P. Véran and G. Herriot, "Woofers-tweeters tip-tilt control for NFIRAOS on TMT," *Proc. SPIE* **6272**, 62721R (2006).
7. K. Avicola, J. A. Watson, B. V. Beeman, T. C. Kuklo, and J. R. Taylor, "Design and performance of the tip-tilt subsystem for the Keck II telescope adaptive optics system," *Proc. SPIE* **3353**, 628–637 (1998).
8. M. S. Belen'kii, "Fundamental limitation in adaptive optics: how to eliminate it? A full-aperture tilt measurement technique with a laser guide star," *Proc. SPIE* **2201**, 321–323 (1994).
9. C. R. Neyman, "Focus anisoplanatism: a limit to the determination of tip-tilt with laser guide stars," *Opt. Lett.* **21**(22), 1806–1808 (1996).
10. R. J. Noll, "Zernike polynomials and atmospheric turbulence," *J. Opt. Soc. Am.* **66**(3), 207–211 (1976).
11. G. A. Tyler, "Bandwidth considerations for tracking through turbulence," *J. Opt. Soc. Am. A* **11**(1), 773340 (1994).
12. B. Sedghi, M. Müller, H. Bonnet, M. Dimmler, and B. Bauvir, "Field stabilization (tip/tilt control) of E-ELT," *Proc. SPIE* **7733**, 401–412 (2010).
13. C. Li, M. Xia, Q. Mu, B. Jiang, L. Xuan, and Z. Cao, "High-precision open-loop adaptive optics system based on LC-SLM," *Opt. Express* **17**(13), 10774–10781 (2009).
14. C. Liu, L. Hu, Q. Mu, Z. Cao, and L. Xuan, "Open-loop control of liquid-crystal spatial light modulators for vertical atmospheric turbulence wavefront correction," *Appl. Opt.* **50**(1), 82–89 (2011).

15. S. Thomas, T. Fusco, A. Tokovinin, M. Nicolle, V. Michau, and G. Rousset, "Comparison of centroid computation algorithms in a Shack–Hartmann sensor," *Mon. Not. R. Astron. Soc.* **371**(1), 323–336 (2006).
16. W. Jiang, H. Xian, and F. Shen, "Detection error of Shack-Hartmann wavefront sensors," *Proc. SPIE* **3126**, 534–544 (1997).
17. V. Voitsekovich, L. Sánchez, and V. Orlov, "Effect of scintillation on adaptive optics systems," *Rev. Mex. Astron. Astrofis.* **38**, 193–198 (2002).
18. F. Mahe, V. Michau, G. Rousset, and J.-M. Conan, "Scintillation effects on wavefront sensing in the Rytov regime," *Proc. SPIE* **4125**, 77–86 (2000).
19. Q. Mu, Z. Cao, L. Hu, Y. Liu, Z. Peng, L. Yao, and L. Xuan, "Open loop adaptive optics testbed on 2.16 meter telescope with liquid crystal corrector," *Opt. Commun.* **285**(6), 896–899 (2012).
20. D. L. Laughlin, D. Rivera, and M. Morari, "Smith predictor design for robust performance," *Int. J. Control* **46**(2), 477–504 (1987).
21. C. Wang, L. Hu, Y. Wang, S. Wang, Q. Mu, D. Li, Z. Cao, C. Yang, H. Xu, and L. Xuan, "Time delay compensation method for tip-tilt control in adaptive optics system," *Appl. Opt.* **54**(11), 3383–3388 (2015).
22. Z. Cao, Q. Mu, L. Hu, Y. Liu, Z. Peng, Q. Yang, H. Meng, L. Yao, and L. Xuan, "Optimal energy-splitting method for an open-loop liquid crystal adaptive optics system," *Opt. Express* **20**(17), 19331–19342 (2012).
23. H. Hu, L. Hu, Z. Peng, Q. Mu, X. Zhang, C. Liu, and L. Xuan, "Advanced single-frame overdriving for liquid-crystal spatial light modulators," *Opt. Lett.* **37**(16), 3324–3326 (2012).

1. Introduction

Adaptive optics system (AOS) has been a compulsory component in many ground-based large aperture optical telescopes to flatten distorted wavefronts and obtain near diffraction-limited resolution images [1–3]. In most AOS, the wavefront correction is divided into two parts [4–6]: a tip tilt mirror (TTM) for correcting the tip-tilt (TT) disturbances and the wavefront corrector (WFC) for the other distortions. Also, the wavefront measurement consists of two parts: a separated sensor for TT detection and other wavefront sensors (WFS) for other distortions [5, 7]. For AOS with laser guide stars (LGS), the laser beacon does not provide TT information because the beam wanders on both the upward and the downward trips through the atmosphere [8, 9], and the separated TT detector is indispensable. For AOS without LGS, the TT detection does not share the WFS with the other distortions because the amplitude of TT is much larger than other distortions. As we know, though TT dominates about 87% of the total atmospheric turbulences [10, 11], this part of TT is relatively small and it cannot exceed the dynamic range of WFS. However, unlike other distortions that are only originated from atmospheric turbulence, many other resources contribute to the TT aberrations, such as dome turbulence in the observatory, mechanical vibrations and imperfect tracking error of the telescope [6, 12]. Furthermore, the alignment between the pupil of telescope and the WFS in AOS is difficult because that the mechanical structure of telescope varies with the different temperatures and pointing elevation angles. And this may induce a large TT to the AOS. The effects of these factors on the TT can be more than an order of magnitude higher than the atmospheric effect. Therefore, such a large amplitude TT often exceeds the normal dynamic range of WFS and separate tip-tilt sensor (TTS) is used in most optical design of the classical AOS without LGS to detect these part of TT. Thus, a part of energy has to be used by TTS. Suppose that if this large TT signal can be obtained from the information detected by WFS, the independent TTS can be moved in the AOS without LGS and this part of energy can be saved to increase the signal-noise-ratio (SNR) of the WFS and imaging CCD. Also, this will simplify the AOS and avoid many mechanical problem.

In this paper, a two-step wavefront measurement method is proposed to measure both large amplitude TT and other distortions with a single Shack-Hartmann WFS (SHWFS). As we know, when the incident light from the telescope is with large amplitude TT, part of incident light cannot reach into the SHWFS and the light spots formed on the CCD are out of their corresponding sub-apertures (subareas). However, the large amplitude TT measurement method in this paper is based on the fact that if we consider the SHWFS as a CCD, the incoming TT disturbance can be estimated from the distribution of these light spots. Thus, the center of gravity of these light spots as a whole can be used to compute the large TT signal. Then the first step pure large TT correction can be conducted using this large TT signal. When the residual TT

decreases to be within the dynamic range of SHWFS, the SHWFS is used for both residual small TT and other distortions' measurement as usual, and the wavefront correction can be normally performed. Compared with the traditional wavefront measurement method, this method saves a TTS, which not only increases the light energy efficiency but also simplifies the AOS.

Section 2 gives the detailed description of this single SHWFS based two-step wavefront measurement method. In section 3, several problems are considered and discussed in the realization of this two-step wavefront detection and correction process, including transition principle between the two steps and control algorithm. Experimental results and analysis on the proposed method and the overall AOS performance are given in section 4. Conclusions are drawn in section 5.

2. Theory

2.1 Two-step wavefront measurement principle

Fig. 1(a) shows the traditional optical structure in our open-loop Liquid crystal AOS (LC-AOS) with a liquid-crystal spatial light modulator as the WFC. In order to improve the energy utilization, unlike closed-loop deformable mirror (DM) AOS, an open-loop control method is adopted for LCWFC control [13, 14]. And a waveband-splitting method is used between the wavefront sensing and imaging. The incident light from telescope is reflected by TTM and then split into two components by a long-wave pass filter LWPFF1. One part with wavelengths less than 500nm is reflected towards a TTS for the large amplitude TT detection. The other part with longer wavelengths passes through LWPFF1 and is further split into two beams by LWPFF2. Then, one beam with wavelengths less than 700 is reflected towards the SHWFS for the measurement of the small amplitude TT and other distortions. The other beam with a longer waveband travels to the LCWFC, and is eventually focused on the imaging CCD.

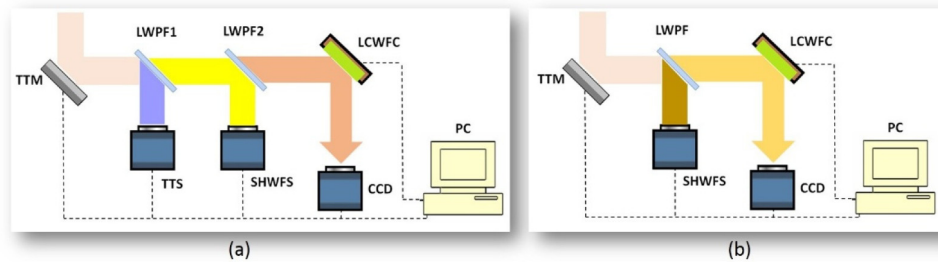


Fig. 1. (a) Schematic diagram of LCAOS with both TTS and SHWFS. (b) LCAOS based on a single SHWFS.

To save energy, the optical design of LC-AOS is changed into one that is shown in Fig. 1(b). The optical branch with the separated TTS is removed, and only the single SHWFS is used to detect both large TT and other distortions. The removing of TTS increases the SNR of SHWFS and imaging CCD and eventually improves the detection ability of the AOS.

When the telescope with the AOS is used for tracking a moving object, the initial TT is so large that the grabbed light spots are not in their corresponding subareas. Since this large TT disables the SHWFS, a TTS as shown in Fig. 1(a) is used to detect the large TT and a rough TT correction is conducted to decrease the TT into the dynamic range of SHWFS in traditional AOS. Here, in the single SHWFS based AOS as shown in Fig. 1(b), a two-step wavefront measurement method is proposed. The first step is the large TT detection by using the SHWFS as a CCD. The second step is the detection for small TT and other distortions by using SHWFS normally.

Considering the adaptive correction process in an AOS, the incident light is with large amplitude TT at the beginning. Therefore, only part of incident light can be captured by

SHWFS and the light spots on SHWFS' CCD are depicted in Fig. 2(a). Obviously, the computed slope in each subarea is wrong and the SHWFS cannot work normally. However, as long as there are light spots on the CCD, from the intensity distribution recorded on each CCD pixel, one can approximately retrieve the global tilt along x and y of the wavefront. That is, when the large TT is out of the dynamic range of SHWFS, the SHWFS is used as a CCD and the center of gravity is used as an estimation of the global TT. Then the rough large TT correction can also be conducted to reduce the residual TT into the dynamic range of SHWFS.

Having completed the first stage of global TT detection and correction, it can move on to the next step. In the second step, the measurement for the small TT and other distortions is the same as it in the traditional SHWFS. After the first rough TT correction, the grabbed light spots array moves into the dynamic range of SHWFS as shown in Fig. 2(b). Each lens produces an image of the object on the 6×6 pixels subarea of the CCD that is denoted by the square. Thus, the average slope of the light spots in every effective subarea of SHWFS is calculated as the small TT and a fine TT correction can be carried out based on it. And the residual slopes subtracting global TT are used to reconstruct wavefront and compute commands for LCWFC. But, it still needs to analyze whether the estimation accuracy of the large global TT signal in the first step is enough to make sure the final residual TT be within the dynamic range of SHWFS. So the following section focuses on the calculation method and precision analysis of the large global TT signal.

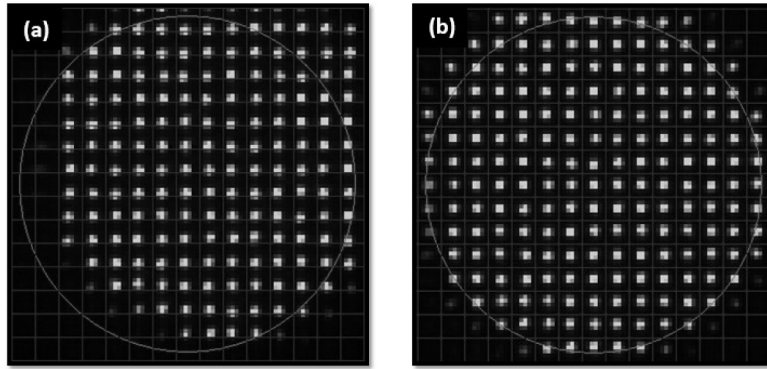


Fig. 2. (a) The object light spots image on the CCD pixel array of SHWFS when the light spots are out of the dynamic range of SHWFS because of the large amplitude TT. (b) Light spots image when TT is within the normal dynamic range of SHWFS.

2.2 Large amplitude global TT detection and precision analysis

As analyzed in section 2.1, when the SHWFS is considered as a CCD, the large global TT denoted as C_{tol} can be derived from the intensity distribution recorded on each CCD pixel. Typically, the center of gravity (CoG) is computed as follows:

$$C_{tol} = \begin{bmatrix} C_{tol,x} \\ C_{tol,y} \end{bmatrix} = \begin{bmatrix} \frac{\sum_{i,j=1}^M x_{i,j} \cdot I_{i,j}}{\sum_{i,j=1}^M I_{i,j}} - Cx_{ref} \\ \frac{\sum_{i,j=1}^M y_{i,j} \cdot I_{i,j}}{\sum_{i,j=1}^M I_{i,j}} - Cy_{ref} \end{bmatrix}. \quad (1)$$

Where, M is the number of pixels on one side of the CCD; Cx_{ref} and Cy_{ref} are the reference centers along x and y directions when the incident light has no TT aberrations, respectively; $x_{i,j}$ and $y_{i,j}$ are the position of the pixel (i, j) along x and y directions, respectively. $I_{i,j}$ is

the corresponding light intensity. $C_{tol,x}$ and $C_{tol,y}$ are the global TT along x and y directions, respectively.

In the field observation, the accuracy of this TT calculation method inevitably suffers from many factors [15–18]. It is difficult to accurately compute the estimation error of the large TT signal in theory. Therefore, simulation is performed for the estimation accuracy of the large TT signal.

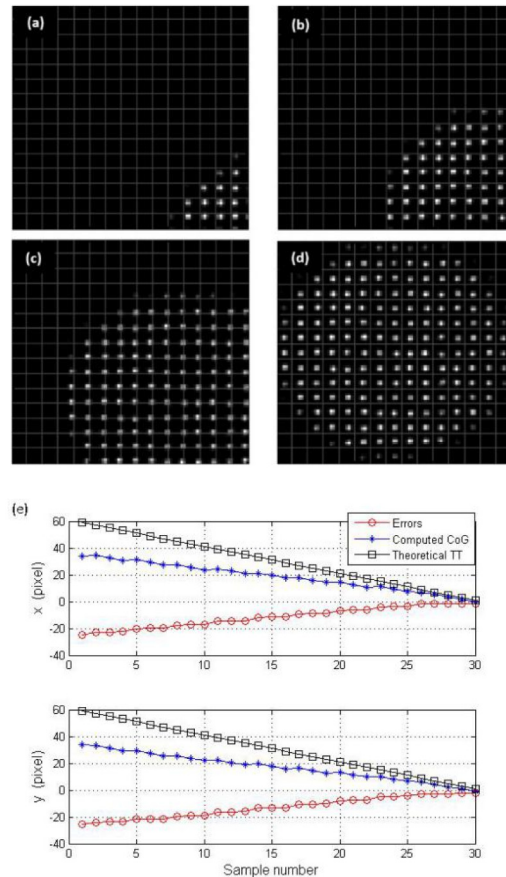


Fig. 3. (a)-(d) show the light spots images recorded on the CCD pixels corresponding to different incoming large TT. (e) Theoretical TT and computed CoG variation with the decreasing of incoming large TT. The red circle line shows the estimation errors. A pixel corresponds to the wavefront distortion of 20λ .

Obviously, at first only a small portion of the incident light can be captured by the SHWFS and the CoG is of low precision to estimate the large TT signal. Yet in an adaptive correction process, the residual TT is decreasing with the first rough TT correction going on. So more incident light can be captured by CCD, and the estimation accuracy increases. To validate this analysis, a simulation is performed with the given incoming TT distortions decreasing along x and y directions simultaneously. Theoretically, the given TT should decrease from both 60 pixels along x and y directions to both 0 pixels. And at each sampling period, the TT decrease 2 pixels in each direction. Figures 3(a)-3(d) plot several typical light spots images recorded on CCD pixels. If the light spots is considered as a whole, the theoretical displacement positions corresponding these four typical images are (60, 60), (40, 40), (20, 20), (0, 0) respectively. Figure 3(e) compares the computed CoG using Eq. (1) with the theoretical TT along x and y directions in every sampling period. And the red line illustrates that the variation in the large TT

estimation errors when the incoming TT is decreasing. When the theoretical TT is both 2 pixels along x and y directions, all light spots move into their corresponding subareas and the estimation errors are 0.58 pixels and 0.62 pixels in x and y direction respectively. When the theoretical TT is zero as shown in Fig. 3(d), the estimation errors along x and y directions are 0.3 pixels and 0.24 pixels respectively.

According to the simulation results, we can conclude that during the first rough TT correction process, both the residual TT and large TT estimation error are decreasing. Generally, if the estimation error of large global TT can be reduced to be within the dynamic range of SHWFS during this process, with a proper controller, every light spot can be moved into its own subarea after rough TT correction. In our AOS, the size of each light spot and subarea is 2×2 pixels and 6×6 pixels, and the dynamic range of SHWFS is ± 2 pixels. As simulation results shown, the large TT estimation errors are both less than 1 pixel in x and y directions when the residual TT is less than 2 pixels in each direction. So the large TT estimation accuracy is high enough to switch from the first step to the second for the two-step wavefront measurement and correction.

3. Two-step wavefront measurement realization

3.1 Transition principle

In order to realize the two-step wavefront measurement and correction process, a critical problem is the transition criterion between these two stages. Here an optimized double threshold method is introduced to solve this problem. The double threshold principle is described in Fig. 4 with Th_1 and Th_2 the two threshold values. If it is in the first rough TT correction process and the large TT is reduced to be smaller than Th_1, transfer to the second step for small TT and other distortions' detection and correction as the blue line shown in Fig. 4. While, as the red line depicted, the opposite transition occurs if the abrupt incoming TT disturbances make the C_{tol} to be larger than Th_2. The two thresholds are set according to the dynamic range of SHWFS and estimation accuracy of the large TT signal.

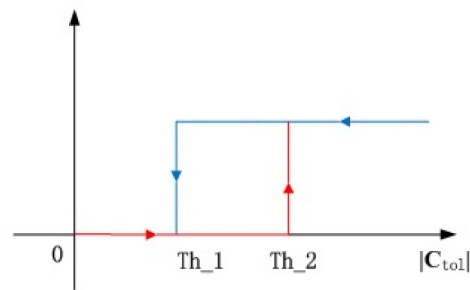


Fig. 4. Double threshold principle for state transition.

3.2 Control algorithm

To achieve the required performance of AOS, TTM and LCWFC should be managed by an efficient control scheme. The control strategy for LCWFC to compensate the other distortions is open-loop control, and the wavefront reconstruction method, influence matrices measurement and feed forward LCWFC controller are all the same as they were conducted in our traditional AOS [14, 19]. But the control algorithm for TTM should be designed separately corresponding to the two steps because of their different tracking precision requirement, TT distortion and measurement noise characteristic.

Typically, the large TT often varies slowly and the detection error is relatively large. Furthermore, the rough TT tracking performance requirement is low. So the conventional simple integrator is a good choice for its simplicity and good stability. As for the small TT

during the second step, in order to obtain good TT tracking performance, Smith predictive compensator is introduced to compensate the pure time delay engendered by wavefront sampling and data processing [20, 21]. The overall control block diagram of the LC-AOS is given in Fig. 5. In addition, the double threshold principle mentioned in section 3.1 is used to decide which controller is used for the current TTM control loop. The ‘Lag’ block in Fig. 5 indicates the system time lag. The incoming wavefront and the TT correction from TTM are denoted as ϕ^{tur} and ϕ^{cor_TT} , respectively.

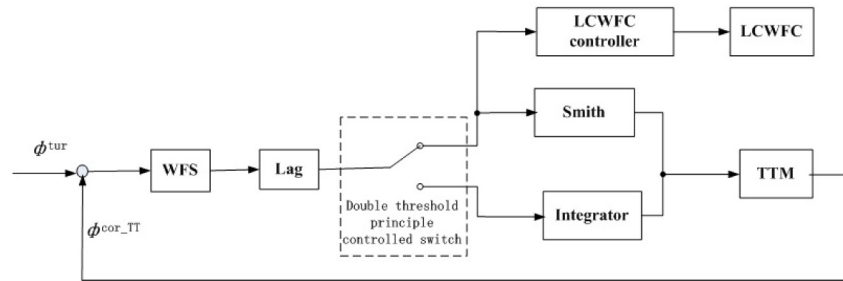


Fig. 5. Control block diagram for the single-sensor based open-loop LC-AOS.

4. Experiment and results

4.1. Experiments in Lab

An optics layout for the single-sensor based LC-AOS is shown in Fig. 6. An atmospheric turbulence simulator (ATS) is placed at the entrance pupil between L1 and L2 to introduce the initial turbulence wavefront. It is a phase plate from the Lexitek Inc, US. The beam with diameter of 1cm through it corresponds to one meter aperture telescope. While a TTM1 is used to generate the large TT and it is conjugated to the ATS by two lenses L2 and L3. The object light reflected by mirror 1 (M1) is collimated using lens L1 and disturbed by ATS, and then reflected by TTM1 that is conjugated to the tip tilt corrector (TTM2) by lenses L4 and L5. The light reflected from TTM2 is split into two beams using a LWPf in such a way that the beam with the short waveband in the range of 400 nm to 700 nm is reflected and zoomed by L6 and L7 towards the SHWFS, and the other beam with the long waveband in the range of 700 nm to 900nm passes through the LWPf and is zoomed using L8 and L9 [22]. The PBS is placed in front of the LCWFC to polarize the beams for correction. The corrected beam reflected by LCWFC is zoomed by L9 and L10 and eventually imaged on the science camera using L11. SHWFS is based on an OCAM2 camera with 120×120 pixels and a 20×20 lenslets array, but in the experiment we only use the 15×15 lenslets array and 90×90 pixels. Thus, each lens corresponds to a subarea of 6×6 . In addition, the focal length of lenslets is 19.35 mm and the pixel size is $48\mu\text{m}$. So the beam diameter on SHWFS is 4.32 mm and a pixel corresponds to the wavefront distortion of 20λ , given the observation wavelength is 550 nm. According to the optical design, the image size is 2×2 and then the normal dynamic range of SHWFS is ± 2 pixels which corresponds to about $\pm 40\lambda$. The two tip tilt mirrors are all from Physik Instrument (PI) Company. The LCWFC is based on the LCOS with pixels of 256×256 from USA BNS Inc. With the over-driving technique [23], the response time of the LCWFC is decreased to about 1ms. The UK Andor DU897 with pixels of 512×512 is used as the imaging science camera.

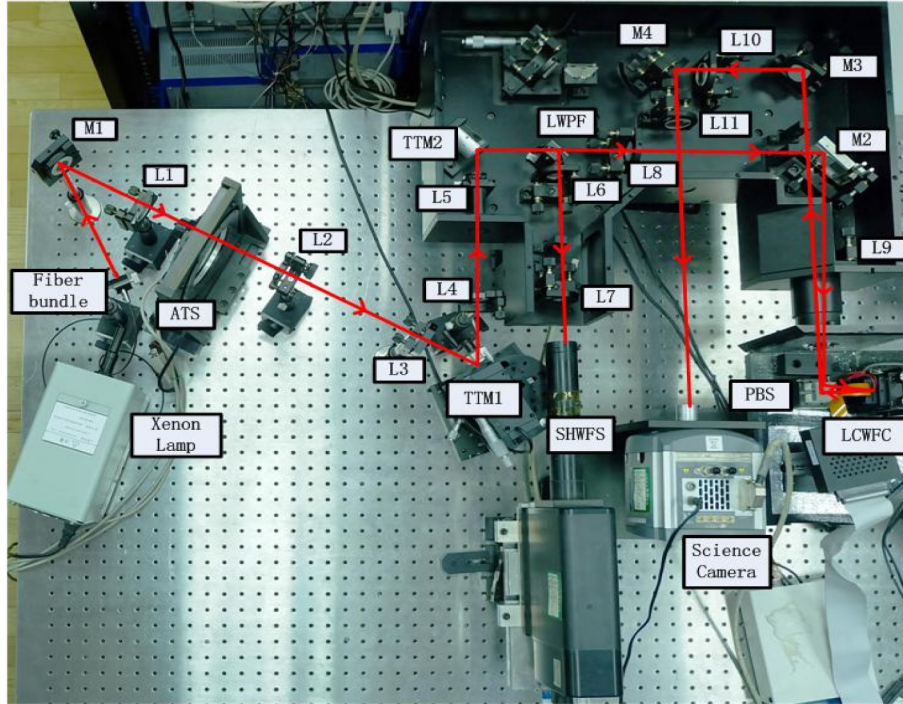


Fig. 6. Photo of the experimental layout for the single-sensor based LC-AOS in lab. M1~M4: mirrors, ATS: atmospheric turbulence simulator, L1~L11: lens.

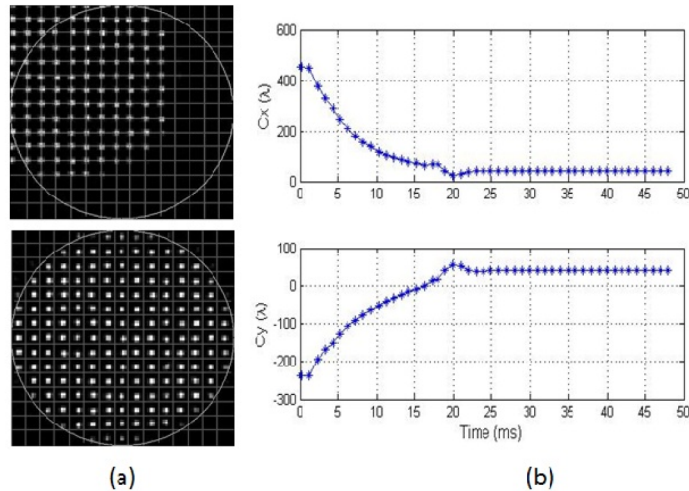


Fig. 7. Static correction results. (a) Lights spots moving process during correction (see Visualization 1). Top: before correction; bottom: after correction. (b) TT variation as a function of time during correction process. A pixel corresponds to 20λ .

The static TT correction results are shown in Fig. 7 with (a) the visualization of light spots moving process detected by SHWFS. During the TT correction process, the TT is measured and depicted in Fig. 7(b). The TT aberrations along x and y directions are reduced from 21 and 14 pixels to less than 0.005 pixels. Considering that a pixel corresponds to the wavefront distortion of 20λ , the residual tip and tilt distortions after correction are both less than 0.1λ . As shown in Fig. 7(a), the light spots is obviously out of the dynamic range of SHWFS before correction.

And the global TT is removed after correction. However, obvious high order distortions still exist in the light spots captured by SHWFS because SHWFS is blind to the LCWFC in our open-loop optical layout.

In addition, a dynamic adaptive correction experiment is performed to validate the ability of this single-sensor based AOS to detect and correct both dynamic large TT and higher-order modes wavefront distortions. The ATS generates an atmospheric turbulence with the Greenwood frequency of 50 Hz and the atmospheric coherence length of 8 cm. TTM1 is excited by a sinusoidal voltage signal to generate the dynamic large TT. The period of the sinusoidal signal is 2 s with the sampling rate of the WFS 1 kHz. In the experiment, the normal dynamic range of SHWFS is ± 2 pixels and the two thresholds Th_1 and Th_2 are set to be 1.6 and 2.5 pixels, respectively. Fig. 8(a) gives the TT aberrations detected by SHWFS along x and y directions before and after correction. After detection, the TT along x and y directions are all reduced from more than 3 pixels rms to 0.01 pixels rms. So the residual tip and tilt distortions are both about 0.2λ rms. The exposure time of the science camera is 10 ms and 50 frames are recorded before and after adaptive correction respectively. The images before and after correction are shown in Fig. 8(b). And the images variation of 100 frames is given in [Visualization 2](#). Obviously, after correction, the image of fiber bundle can be resolved. This dynamic correction result validates that single-sensor based AOS is effective for correcting both large TT and other wavefront distortions.

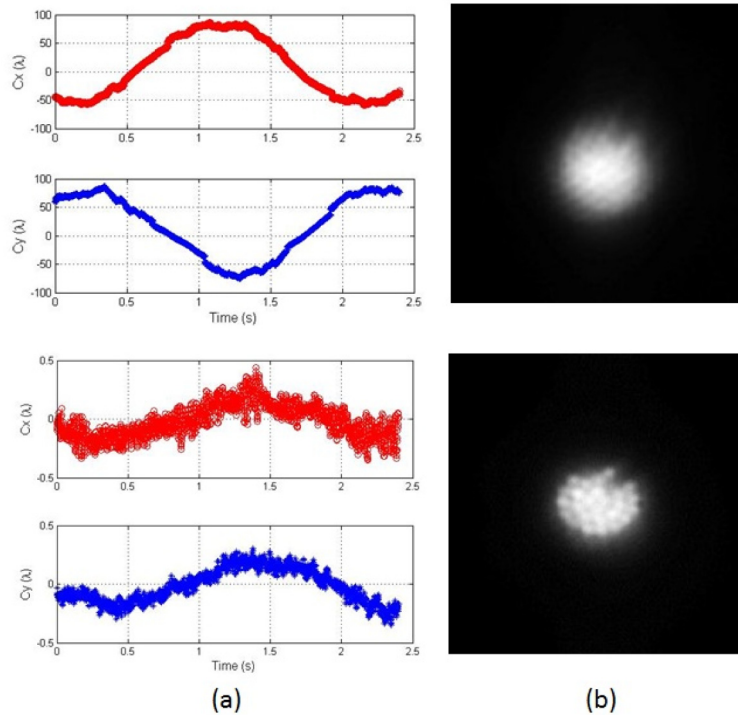


Fig. 8. Dynamic AO correction results. (a) Displacements along x and y directions on SHWFS. Top: before correction; bottom: after correction. A pixel corresponds to 20λ . (b) Fiber bundle images of 100 frames recorded on the imaging CCD during correction (see [Visualization 2](#)). Top: before correction; bottom: after TT correction.

4.2. Observation results on a 1.23m telescope

For the 1.23-meter telescope (CIOMP, China), the theoretical resolution θ_0 is $0.16''$ according to the center observation wavelength 800nm and the aperture of telescope 1.23m. To estimate the resolution of our AOS, several errors need to be considered: 1) the truncated error: limited

Zernike modes are used to correct the turbulence; 2) the fitting error: the liquid crystal corrector cannot exactly produce the shape of Kolmogorov turbulence; 3) the temporal error due to the time delay in control system; 4) the noise error: the wavefront sensor makes exact measurement impossible. Given that the atmospheric coherence length of 7 cm, the Greenwood frequency of 45Hz, the number of Zernike modes used in correction of 65, the wavelength of 0.550 μm , the number of quantization levels for the liquid crystal corrector of 16, the SNR of 20, the Strehl ratio is estimated to be about 0.21 at the telescope site in our institute. Therefore, the estimated resolution of our AOS is about 0.35".

As for the TT correction, unlike a common telescope with AOS that has two tilt tip mirrors for rough tracking and fine tracking respectively, the 1.23m telescope with our LC-AOS has only one tilt tip mirror in total. The maximum tracking error of the telescope is less than 10λ for tracking a star, which is obviously within the dynamic range of SHWFS. However, the alignment error between the telescope and the AOS often lead to a large TT to the AOS. Its amplitude depends on the environment temperature and the pointing elevation angle and can reach 100λ which often makes the pupil shift outside the SHWFS. In addition, when tracking a moving objects, the tracking error mainly depends on the speed of the observation objects and this TT can often exceeds the dynamic range of the SHWFS according to our experience.

An adaptive correction experiment was performed. The Greenwood frequency and atmospheric coherence length are measured as 45 Hz and 7 cm, respectively. The observation object is a binary star (5.16mag, 4.87mag, theoretical angle distance of 0.6") named as TDSC41102. The sampling frequency of WFS is 930 Hz, and the exposure time of imaging science camera is 356ms. The image of the binary stars with and without adaptive correction are shown in Figs. 9(a) and 9(b), respectively.

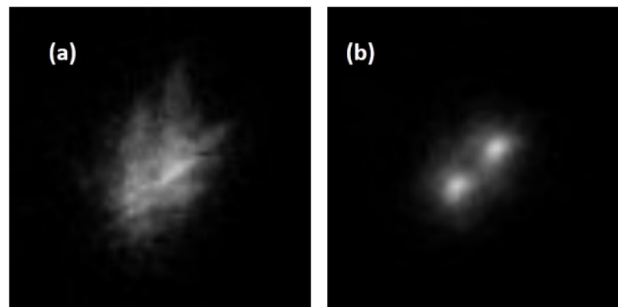


Fig. 9. Observation results of a double-star TDSC41102 on 1.23m AO telescope. (a) Before correction. (b) After correction.

5. Conclusion

This paper is mainly talking about an energy saving adaptive optical layout which saves the traditional separated tip-tilt sensor and detects the large amplitude TT and other distortions based on a single Hartmann-Shack wavefront sensor. And in this paper a two-step wavefront measurement method is presented to realize the detection for both large TT and other distortions with a single SHWFS. The lab adaptive correction results verify the proposed method. The experiments on a 1.23-meter optical telescope indicates that the binary stars with angle distance of 0.6" are clearly resolved with our AOS, which further validates the wavefront detection and correction ability of our single-sensor based AOS.

As the separated TTS seems to be a classic setup in traditional AOS without LGS in astronomical applications for more than 30 years, our method indicates an effective way to optimize the traditional optical layout in adaptive optics. By doing this way the AOS is simplified which can avoid the cost and many other mechanical problem. Furthermore, the proposed method saved light throughput for imaging and wavefront sensing, which means a higher SNR for the WFS and makes it promising to be used to improve the detection capability

of the AOS. In addition, it will be helpful if our method may motivate readers to do some changes in their applications, such as laser communications, laser power, retinal imaging, and adaptive optics microscope and so on. While, the only disadvantage is its complex data process technique which is not a challenge at all.

Acknowledgments

This work is supported by the National Natural Science Foundation of China, with Grant Nos. 61205021, 61377032, and 61475152.